

Exploring and predicting intermolecular binding preferences in crystalline Cu(II) coordination complexes

Ivan Kodrin, Mladen Borovina, Luka Šmital, Jesús Valdés-Martínez, Christer B. Aakeröy,
Marijana Đaković

Department of Chemistry, Faculty of Science, University of Zagreb, Zagreb, Croatia

*Instituto de Química, Universidad Nacional Autónoma de México, Circuito Exterior, Ciudad
Universitaria, México, D. F. México*

Department of Chemistry, Kansas State University, Manhattan, KS, 66506, USA

Supplementary information

Table of Contents

1. Single crystal X-ray crystallography	3
2. Powder X-ray crystallography	12
3. Hirshfeld surfaces.....	17
4. Interaction energies of the short-range interactions	19
5. Comparison of interaction energies calculated at different levels of theory	23

1. Single crystal X-ray crystallography

Table S1. Crystal data and details of the structure determination for **1a – 5a**.

Compound	1a	2a	3a	4a
Formula	C ₂₂ H ₁₄ CuF ₁₂ N ₄ O ₆	C ₂₄ H ₁₈ CuF ₁₂ N ₄ O ₆	C ₂₂ H ₁₄ CuF ₁₂ N ₄ O ₆	C ₂₄ H ₁₈ CuF ₁₂ N ₄ O ₆
M_r	721.91	749.96	721.91	749.96
Colour and habit	green, block	green, block	green, block	green, block
Crystal system, space group	Triclinic, $P\bar{1}$	Triclinic $P\bar{1}$	Triclinic, $P\bar{1}$	Triclinic $P\bar{1}$
Crystal dimensions (mm ³)	0.04 x 0.11 x 0.26	0.10 x 0.15 x 0.35	0.25 x 0.41 x 0.43	0.35 x 0.50 x 0.55
a (Å)	8.7980(14)	8.5710(4)	6.9635(12)	6.7979(6)
b (Å)	9.4558(18)	8.6068(5)	10.0912(14)	10.8757(6)
c (Å)	9.9430(15)	10.9486(6)	10.3229(16)	11.5285(8)
α (°)	86.776(15)	96.577(5)	69.049(14)	117.344(6)
β (°)	73.162(14)	106.692(5)	80.726(14)	90.254(7)
γ (°)	63.012(18)	102.284(5)	83.957(14)	98.312(6)
V (Å ³)	702.8(2)	742.49(7)	667.68(19)	746.70(10)
Z	1	1	1	1
T (K)	296 (2)	296 (2)	296 (2)	296 (2)
D_{calc} (g cm ⁻³)	1.706	1.677	1.795	1.668
μ (mm ⁻¹)	0.901	0.856	0.949	0.852
$F(000)$	359	375	359	375
θ range for data collection (°)	3.80 – 25.98	3.71 – 28.00	3.42 – 27.00	3.55 – 25.00
h, k, l range	-7:10, -11:11, -12:12	-11:11, -11:11, -14:14	-8:8, -12:12, -12:13	-8:6, -12:12, -12:13
Scan type	ω	ω	ω	ω
No. measured reflections	6111	7122	6284	5527
No. independent reflections (R_{int})	2755 (0.0379)	3594 (0.0193)	2896 (0.0264)	2604 (0.0317)
No. observed reflections, $I \geq 2\sigma(I)$	1978	2846	2502	2054
No. refined parameters	262	247	237	247
$R, wR [I \geq 2\sigma(I)]$	0.0704, 0.1761	0.0421, 0.1037	0.0461, 0.1261	0.0467, 0.0989
R, wR [all data]	0.0997, 0.1927	0.0572, 0.1112	0.0551, 0.1309	0.0681, 0.1078
Goodness of fit on F^2, S	1.042	1.039	1.119	1.028
Max., min. electron density (e Å ⁻³)	-0.240, 1.145	-0.304, 0.455	-0.267, 0.940	-0.214, 0.219
CCDC number	1942720	1942721	1942723	1942725

Compound	5a-I	5a-II
Formula	C ₃₄ H ₂₂ CuF ₁₂ N ₄ O ₆	C ₃₄ H ₂₂ CuF ₁₂ N ₄ O ₆
<i>M_r</i>	874.09	874.09
Colour and habit	Green, block	Green, block
Crystal system, space group	Triclinic, <i>P</i> $\bar{1}$	Monoclinic <i>P</i> 2 ₁ / <i>c</i>
Crystal dimensions (mm ³)	0.21 x 0.25 x 0.39	0.20 x 0.23 x 0.31
<i>a</i> (Å)	9.0451(4)	11.3294(5)
<i>b</i> (Å)	10.1886(5)	22.7479(6)
<i>c</i> (Å)	10.3628(4)	7.3599(3)
α (°)	105.030(4)	90
β (°)	97.391(4)	103.836(4)
γ (°)	93.535(4)	90
<i>V</i> (Å ³)	910.16(7)	1841.76(12)
<i>Z</i>	1	2
<i>T</i> (K)	296(2)	296(2)
<i>D</i> _{calc} (g cm ⁻³)	1.595	1.576
μ (mm ⁻¹)	0.712	0.703
<i>F</i> (000)	439	878
θ range for data collection (°)	2.84 – 28.00	3.14 – 26.00
<i>h,k,l</i> range	–11:11, –13:13, –13:13	–13:13, –26:28, –9:9
Scan type	ω	ω
No. measured reflections	8348	8821
No. independent reflections (<i>R</i> _{int})	4385 (0.0237)	3611 (0.0346)
No. observed reflections, <i>I</i> ≥ 2σ(<i>I</i>)	3731	2879
No. refined parameters	291	299
<i>R</i> , w <i>R</i> [<i>I</i> ≥ 2σ(<i>I</i>)]	0.0432, 0.1118	0.0431, 0.1063
<i>R</i> , w <i>R</i> [all data]	0.0530, 0.1183	0.0570, 0.1136
Goodness of fit on <i>F</i> ² , <i>S</i>	1.036	1.058
Max., min. electron density (e Å ⁻³)	–0.424, 0.479	–0.333, 0.315
CCDC number	1942727	1942728

Table S2. Crystal data and details of the structure determination for **2b** – **5b**.

Compound	2b	3b	4b	5b
Formula	C ₂₄ H ₂₄ CuF ₆ N ₄ O ₆	C ₁₆ H ₁₄ CuF ₆ N ₂ O ₅	C ₂₄ H ₂₄ CuF ₆ N ₄ O ₆	C ₃₄ H ₂₈ CuF ₆ N ₄ O ₆
M_r	642.01	491.83	642.01	766.14
Colour and habit	green, block	green, plate	green, block	green, prism
Crystal system, space group	Tetragonal <i>P4₁2₁2</i>	Monoclinic <i>P2₁/n</i>	Triclinic <i>P$\bar{1}$</i>	Monoclinic, <i>P2₁/n</i>
Crystal dimensions (mm ³)	0.22 x 0.27 x 0.40	0.11 x 0.21 x 0.49	0.20 x 0.25 x 0.50	0.35 x 0.42 x 0.66
<i>a</i> (Å)	8.9094(2)	6.7411(3)	8.5478(4)	10.3647(2)
<i>b</i> (Å)	8.9094(2)	15.9660(8)	9.2084(4)	9.6311(2)
<i>c</i> (Å)	33.9781(12)	18.5837(6)	10.0669(5)	17.9637(5)
α (°)	90	90	114.584(4)	90
β (°)	90	94.453(3)	99.527(4)	100.920(2)
γ (°)	90	90	98.514(4)	90
<i>V</i> (Å ³)	2697.09(15)	1994.10(15)	689.52(6)	1760.7(7)
<i>Z</i>	4	4	1	2
<i>T</i> (K)	200 (2)	296 (2)	296 (2)	296(2)
D_{calc} (g cm ⁻³)	1.581	1.638	1.546	1.445
μ (mm ⁻¹)	0.898	1.180	0.878	0.701
<i>F</i> (000)	1308	988	327	782
θ range for data collection (°)	3.31 – 29.00	3.29 – 25.50	3.53 – 26.00	3.27 – 27.50
<i>h,k,l</i> range	–7:12, –9:10, –46:38	–8:8, –19:18, –20:22	–10:10, –11:11, –12:12	–13 : 13, –12 : 12, –23 : 23
Scan type	ω	ω	ω	ω
No. measured reflections	7762	8392	10981	33584
No. independent reflections (R_{int})	3587 (0.0298)	3705 (0.0328)	2713 (0.0271)	4050 (0.0306)
No. observed reflections, $I \geq 2\sigma(I)$	3223	2790	2552	3572
No. refined parameters	192	333	221	265
Flack parameter (<i>x</i>)	0.003(8)	-	-	-
<i>R</i> , wR [$I \geq 2\sigma(I)$]	0.0413, 0.0985	0.0495, 0.1340	0.0336, 0.0922	0.0329, 0.0860
<i>R</i> , wR [all data]	0.0488, 0.1035	0.0693, 0.1484	0.0369, 0.0952	0.0385, 0.0897
Goodness of fit on F^2 , <i>S</i>	1.056	1.047	1.104	1.081
Max., min. electron density (e Å ⁻³)	–0.251, 0.353	–0.307, 0.841	–0.228, 0.243	–0.356, 0.285
CCDC number	1942722	1942724	1942726	1942729

Table S3. Selected bond distances (Å) and angles (°) for **1a**, **2a**, **3a**, **4a**.

	1a	2a	3a	4a
Cu1–O1	2.010(3)	2.030(2)	1.971(2)	2.023(2)
Cu1–O2	2.301(3)	2.246(2)	2.334(2)	2.266(2)
Cu1–N1	2.017(4)	2.018(2)	2.071(3)	2.049(2)
O1–Cu1–O2	84.88(12)	86.95(6)	85.32(8)	86.39(8)
O1–Cu1–O2 ^{<i>i</i>}	95.12(12)	93.05(6)	94.68(8)	93.61(8)
O1–Cu1–N1	89.67(14)	89.73(8)	90.77(9)	90.41(9)
O1–Cu1–N1 ^{<i>i</i>}	90.33(14)	90.27(8)	89.23(9)	89.59(9)
O2–Cu1–N1	93.05(14)	91.17(7)	91.98(9)	89.87(9)
O2–Cu1–N1 ^{<i>i</i>}	86.95(14)	88.83(7)	88.02(9)	90.13(9)

Symmetry codes (*i*): 1–*x*, 1–*y*, 1–*z* (**1a**, **2a**, **3a**, **4a**)**Table S4.** Selected bond distances (Å) and angles (°) for **5a-I**, **5a-II** and **5b**

	5a-I	5a-II	5b
Cu1–O1	1.988(2)	2.041(2)	1.941(1)
Cu1–O2	2.338(2)	2.226(2)	2.217(2)
Cu1–N1	2.009(2)	2.021(2)	2.124(2)
O1–Cu1–O2	84.90(6)	86.97(7)	89.52(5)
O1–Cu1–O2 ^{<i>i</i>}	95.10(6)	93.03(7)	90.48(5)
O1–Cu1–N1	89.56(6)	90.20(8)	90.46(5)
O1–Cu1–N1 ^{<i>i</i>}	90.44(6)	89.80(8)	89.54(5)
O2–Cu1–N1	93.19(6)	91.74(7)	89.45(5)
O2–Cu1–N1 ^{<i>i</i>}	86.81(6)	88.26(7)	90.55(5)

Symmetry codes (*i*): 1–*x*, 1–*y*, 1–*z* (**5a-I**, **5a-II**, **5b**)

Table S5. Selected bond distances (Å) and angles (°) for **2b** – **4b**.

	2b	4b		3b
Cu1–O1	1.959(2)	1.968(2)	Cu1–O1	1.928(3)
Cu1–O2	2.180(3)	2.294(2)	Cu1–O2	1.968(2)
Cu1–N1	2.155(3)	2.053(2)	Cu1–O3	1.972(2)
O1–Cu1–O1 ⁱ	177.50(15)	180	Cu1–O4	1.931(3)
O2–Cu1–O2 ⁱ	81.46(14)	180	Cu1–N1	2.235(3)
N1–Cu1–N1 ⁱ	95.52(14)	180	O1–Cu1–O2	92.56(11)
O1–Cu1–O2	86.92(11)	87.62(6)	O1–Cu1–O3	89.52(11)
O1–Cu1–O2 ⁱ	91.18(10)	92.38(6)	O1–Cu1–O4	165.22(12)
O1–Cu1–N1	90.46(10)	90.37(6)	O2–Cu1–O3	167.06(11)
O1–Cu1–N1 ⁱ	91.22(10)	89.63(6)	O2–Cu1–O4	83.64(11)
O2–Cu1–N1	172.49(10)	91.33(6)	O3–Cu1–O4	91.14(11)
O2–Cu1–N1 ⁱ	91.57(10)	88.67(6)	O1–Cu1–N1	94.71(11)
			O2–Cu1–N1	95.79(11)
			O3–Cu1–N1	96.77(12)
			O4–Cu1–N1	99.87(12)

Symmetry codes (*i*): $-x+1, -y+1, -z+1/2$ (**2b**), $1-x, 1-y, 1-z$ (**4b**)

Table S6. Hydrogen bond geometries for compounds **1a–5b**.

D–H...A	$d(\text{D}\cdots\text{A}) /$	$d(\text{H}\cdots\text{A}) / \text{Å}$	$\angle(\text{D–H}\cdots\text{A}) / ^\circ$	Symmetry operator
[Cu(hfac)₂(3-Hoxpy)₂] (1a)				
O3–H3...O2	2.825(5)	2.02	166	$x-1, y+1, z$
C10–H10...O3	3.483(7)	2.59	162	$x+1, y-1, z$
[Cu(hfac)₂(3-Meoxpy)₂] (2a)				
O3–H3...N2	2.827(3)	2.01(4)	156(4)	$-x, 1-y, -z$
[Cu(tfac)₂(3-Meoxpy)₂] (2b)				
O3–H3...O2	2.764(4)	2.00(3)	158(6)	$2-x, 1-y, 1/2-z$
C9–H9...O3	3.526(5)	2.62	160	$x-1/2, 3/2-y, 3/4-z$
C10–H10...O3	3.200(4)	2.52	128	$x, y-1, z$
[Cu(hfac)₂(4-Hoxpy)₂] (3a)				
O3–H3...N2	2.918(5)	2.18(3)	152(6)	$3-x, -y, 1-z$
C7–H7...O2	3.208(4)	2.39	146	$x+1, y, z$
[Cu(tfac)₂(4-Hoxpy)] (3b)				
O5–H5...O2	3.070(5)	2.28(2)	166(5)	$5/2-x, y+1/2, 3/2-z$
O5–H5...O4	2.873(4)	2.37(5)	121(5)	$5/2-x, y+1/2, 3/2-z$
C14–H14...O3	3.274(5)	2.59	131	$x+1, y, z$
[Cu(hfac)₂(4-Meoxpy)₂] (4a)				
O3–H3...N2	2.827(4)	2.03(1)	167(4)	$-1-x, -y, 1-z$
C7–H7...O2	3.277(4)	2.53	137	$x-1, y, z$
[Cu(tfac)₂(4-Meoxpy)₂] (4b)				
O3–H3...O2	2.751(2)	1.95(1)	177(4)	$x, y+1, z+1$
C5–H5C...O3	3.347(4)	2.56	140	$2-x, 2-y, 2-z$
[Cu(hfac)₂(4-Phoxpy)₂] (5a-I)				
O3–H3...O2	2.859(2)	2.05(2)	170(5)	$1-x, 1-y, 2-z$
[Cu(hfac)₂(4-Phoxpy)₂] (5a-II)				
O3A–H3A...N2	2.818(4)	2.08	149	$-x, 1-y, -1-z$
O3B–H3B...N2	2.771(6)	2.04	149	$-x, 1-y, -1-z$
[Cu(tfac)₂(4-Phoxpy)₂] (5b)				
O3–H3...O2	2.762(2)	1.94(3)	173(3)	$2-x, 1-y, 1-z$
C5–H5B...O3	3.488(3)	2.58	159	$x-1/2, 1/2-y, z+1/2$

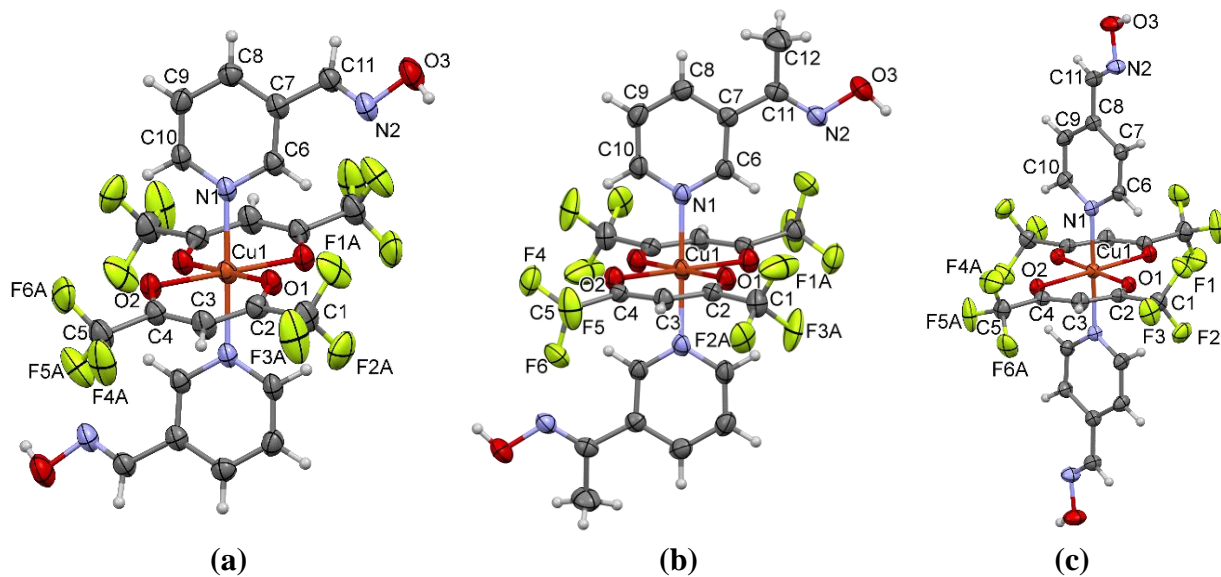


Figure S1. ORTEP-style plot of the two symmetrically independent molecules of: (a) $[\text{Cu}(\text{hfac})_2(3\text{-Hoxy})_2]$ (**1a**), (b) $[\text{Cu}(\text{hfac})_2(3\text{-Meoxy})_2]$ (**2a**), and $[\text{Cu}(\text{hfac})_2(4\text{-Hoxy})_2]$ (**3a**). Thermal ellipsoids are drawn at 30% probability level at 296(2) K.

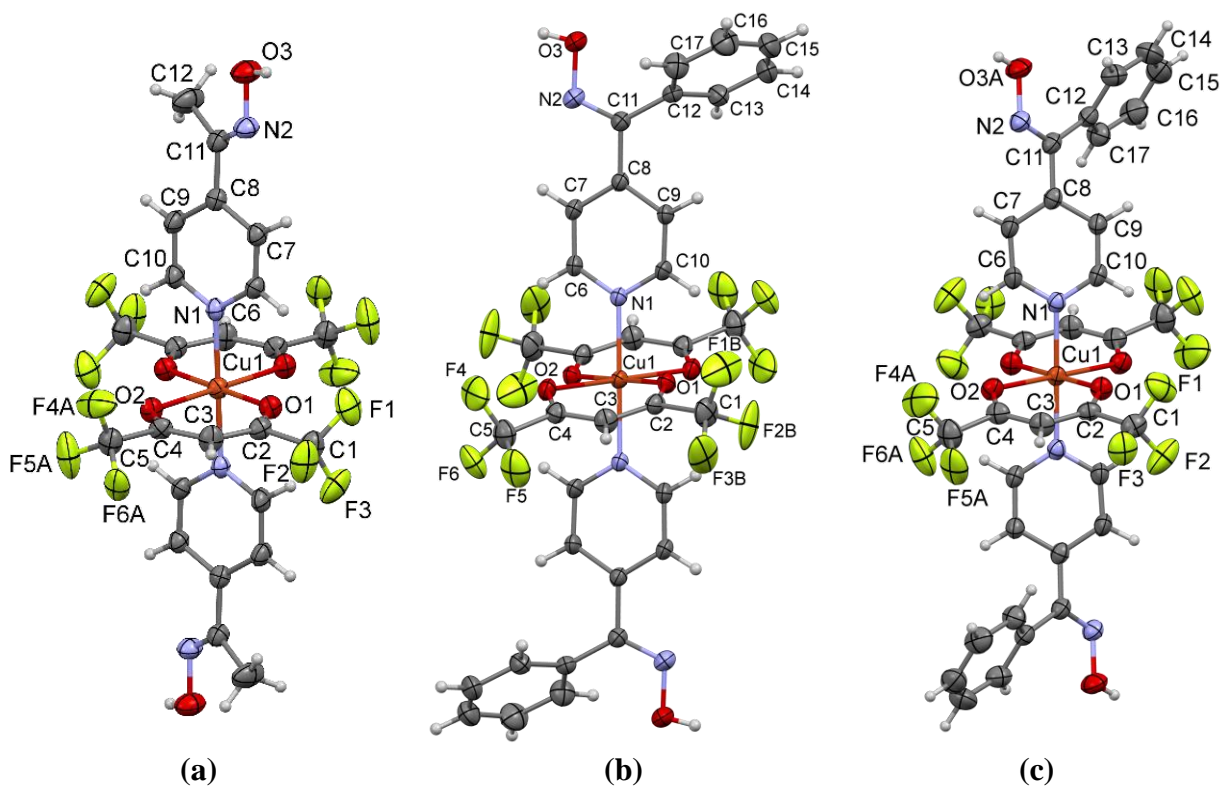


Figure S2. ORTEP-style plot of: (a) $[\text{Cu}(\text{hfac})_2(4\text{-Meoxy})_2]$ (**4a**), (b) $[\text{Cu}(\text{hfac})_2(4\text{-Phoxy})_2]$ (**5a-I**), (c) $[\text{Cu}(\text{hfac})_2(4\text{-Phoxy})_2]$ (**5a-II**). Thermal ellipsoids are drawn at 30% probability level at 296(2) K.

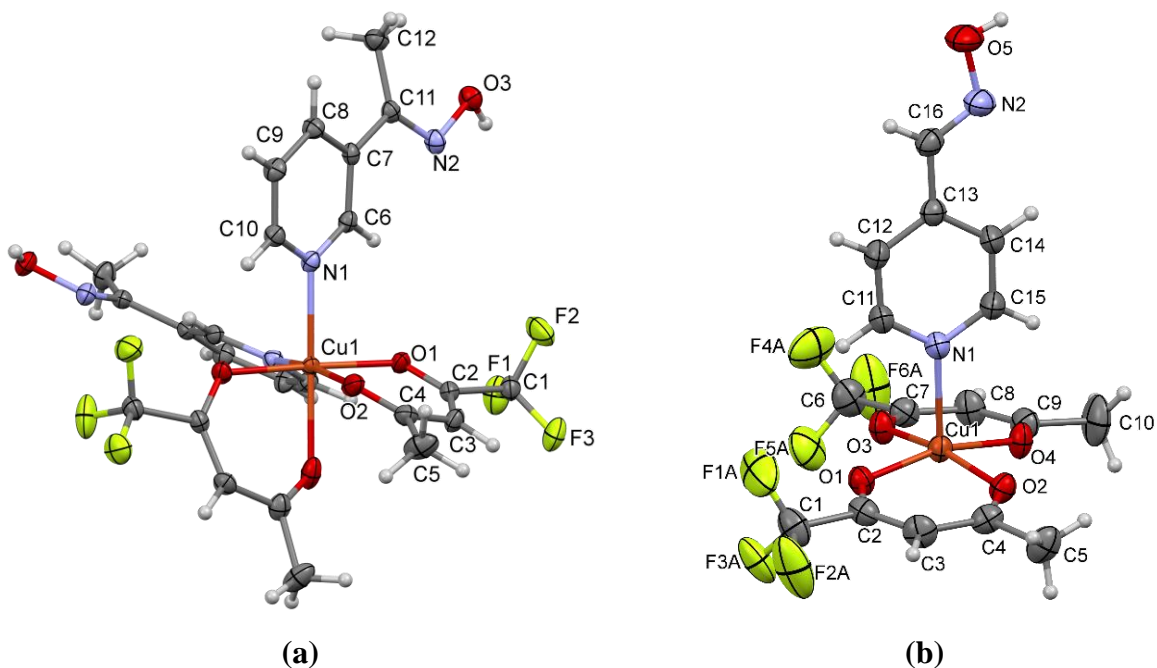


Figure S3. ORTEP-style plot of: (a) $[\text{Cu}(\text{tfac})_2(3\text{-Meoxy})_2]$ (**2b**), (b) $[\text{Cu}(\text{hfac})_2(4\text{-Hoxpy})]$ (**3b**). Thermal ellipsoids are drawn at 30% probability level at 200(2) K (**2b**) and 296(2) K (**3b**).

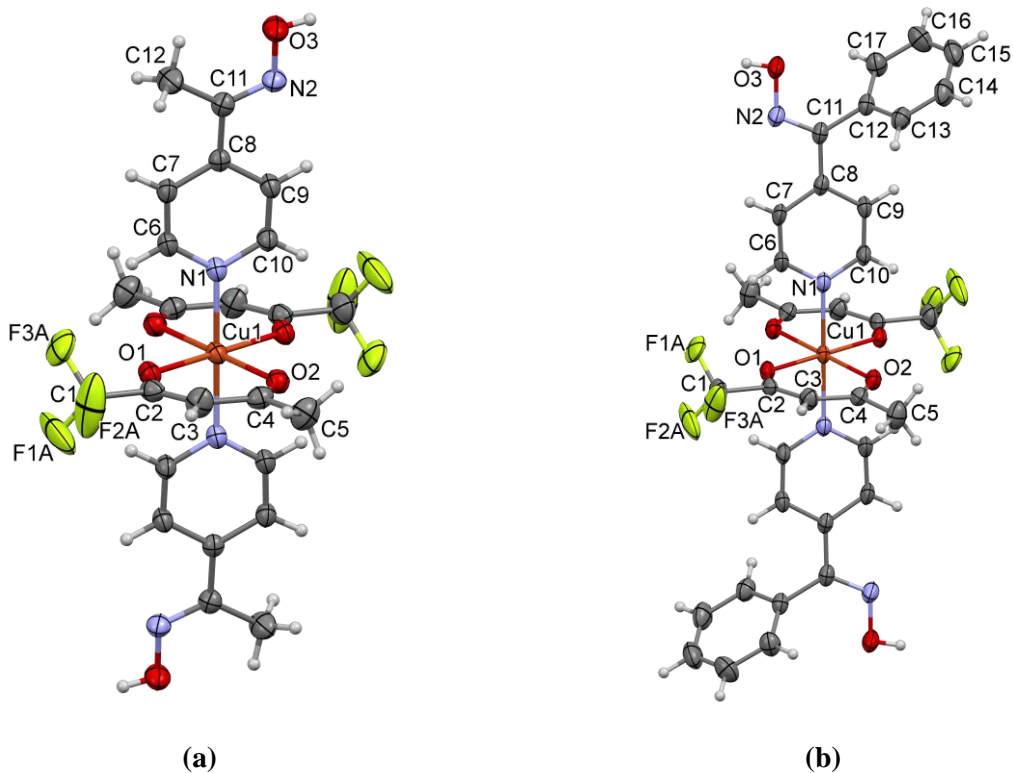


Figure S4. ORTEP-style plot of: (a) $[\text{Cu}(\text{tfac})_2(4\text{-Meoxy})_2]$ (**4b**), (b) $[\text{Cu}(\text{tfac})_2(4\text{-Phoxpy})_2]$ (**5b**). Thermal ellipsoids are drawn at 30% probability level at 296(2) K.

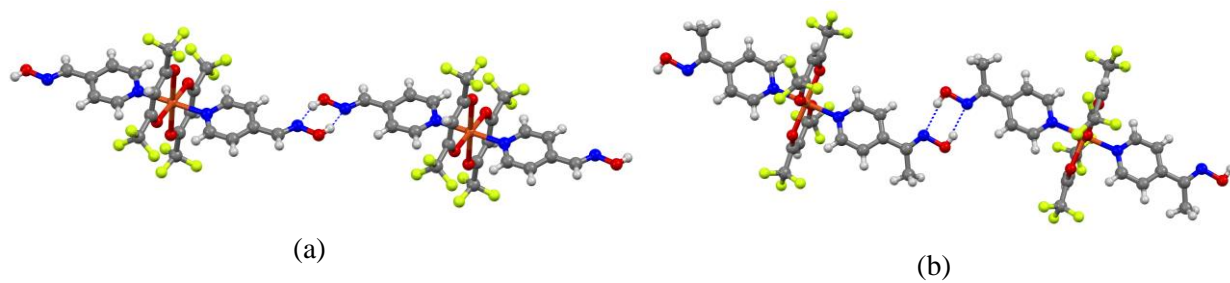


Figure S5. $R_2^2(6)$ supramolecular synthons in the structure of: (a) [Cu(hfac)₂(4-Hoxpy)₂] (**3a**), (b) [Cu(hfac)₂(4-Meoxpy)₂] (**4a**).

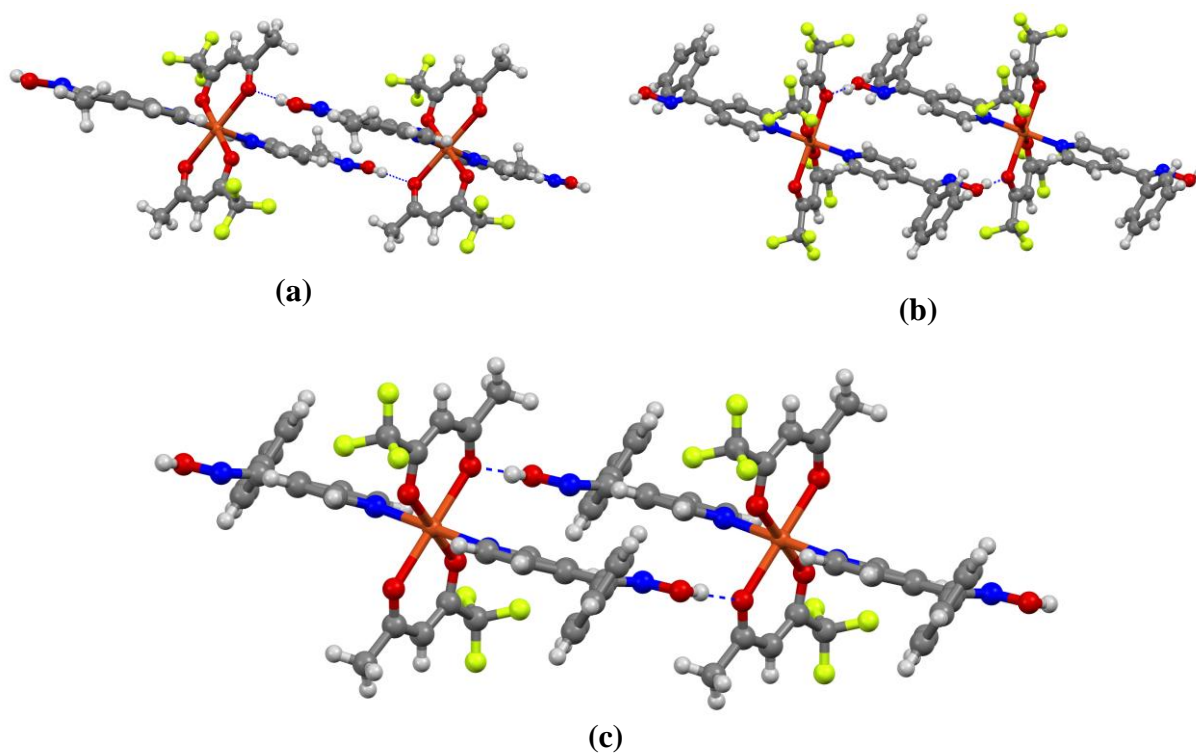


Figure S6. O-H...O_{β-dik} supramolecular synthons in the structure of: (a) [Cu(tfac)₂(4-Meoxpy)₂] (**4b**), (b) [Cu(hfac)₂(4-Phoxpy)₂] (**5a-I**), (c) [Cu(tfac)₂(4-Phoxpy)₂] (**5b**).

2. Powder X-ray crystallography

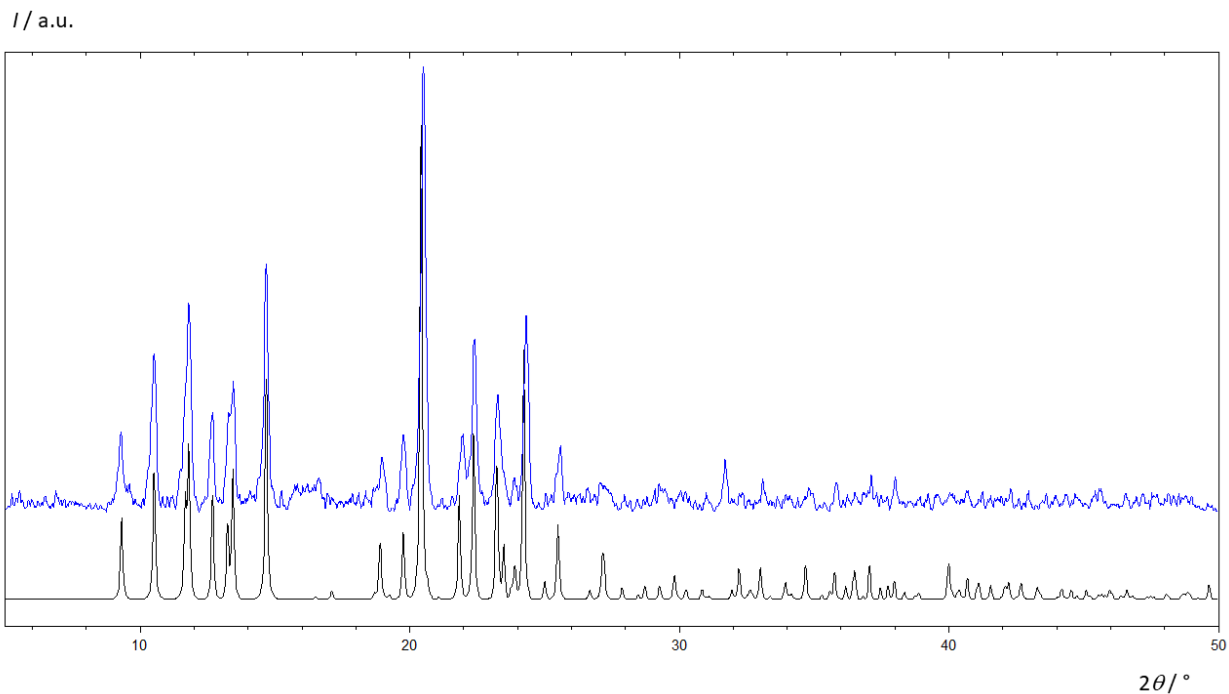


Figure S7. Experimental (**blue**) and calculated (**black**) PXRD traces of $[\text{Cu}(\text{hfac})_2(3\text{-Hoxpy})_2]$ (**1a**)

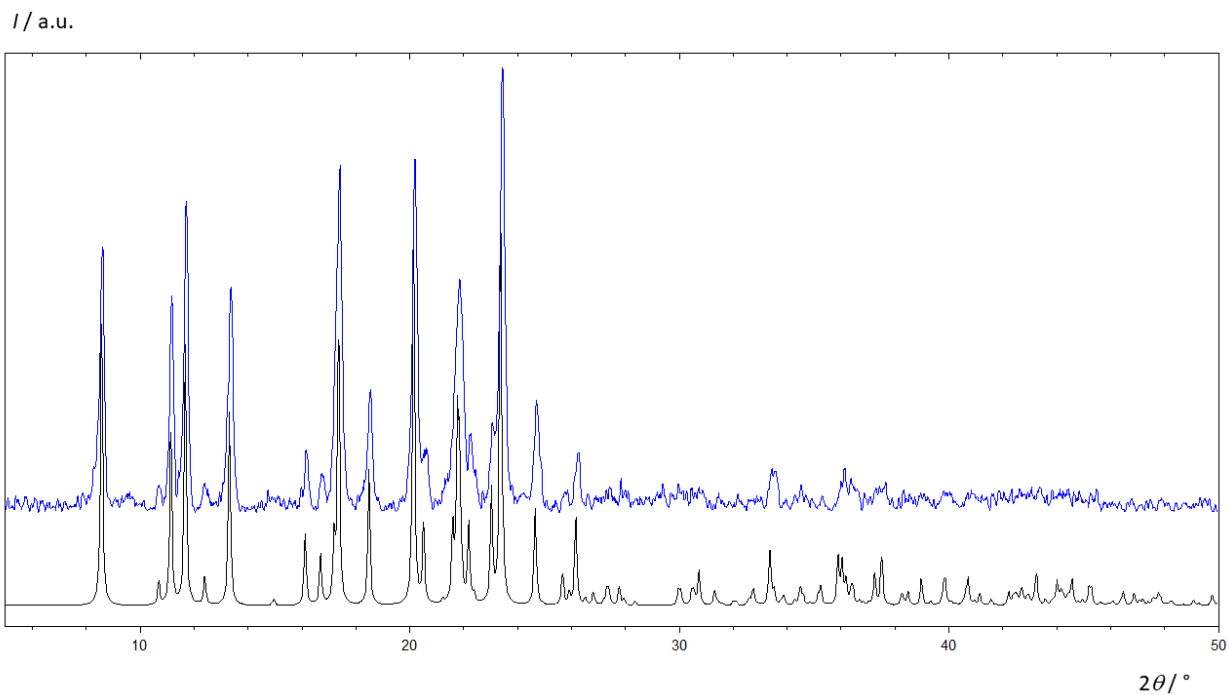


Figure S8. Experimental (**blue**) and calculated (**black**) PXRD traces of $[\text{Cu}(\text{hfac})_2(3\text{-Meoxpy})_2]$ (**2a**)

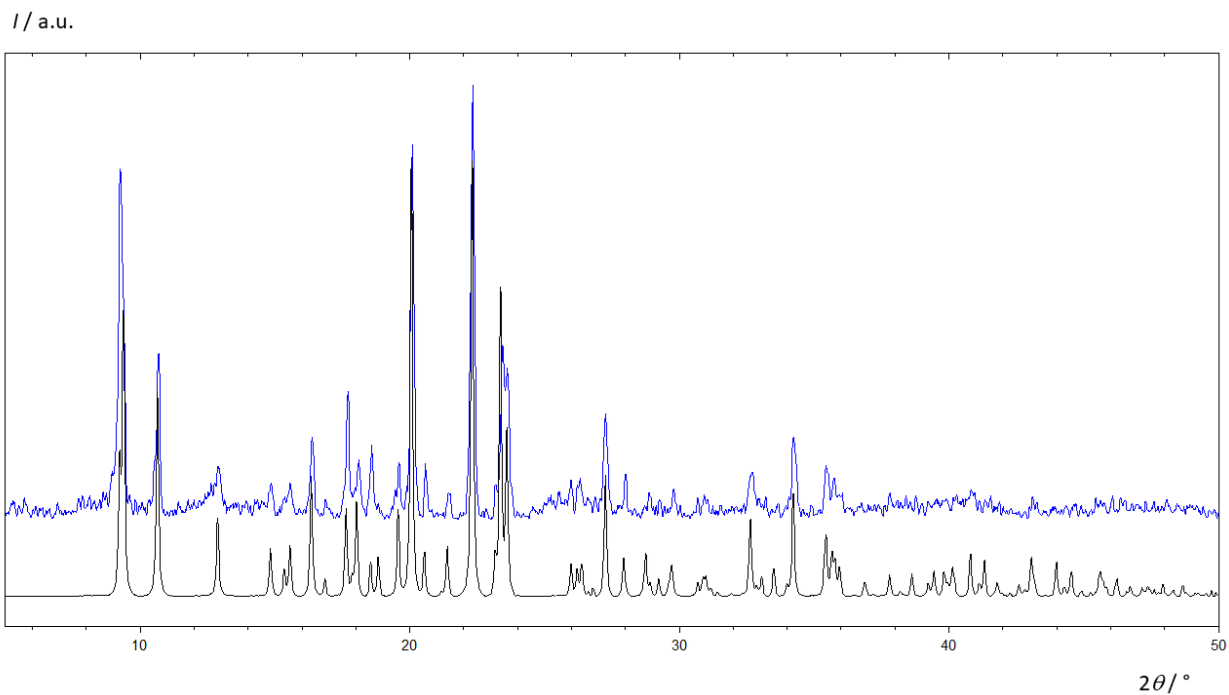


Figure S9. Experimental (**blue**) and calculated (**black**) PXR D traces of $[\text{Cu}(\text{hfac})_2(4\text{-Hoxpy})_2]$ (**3a**)

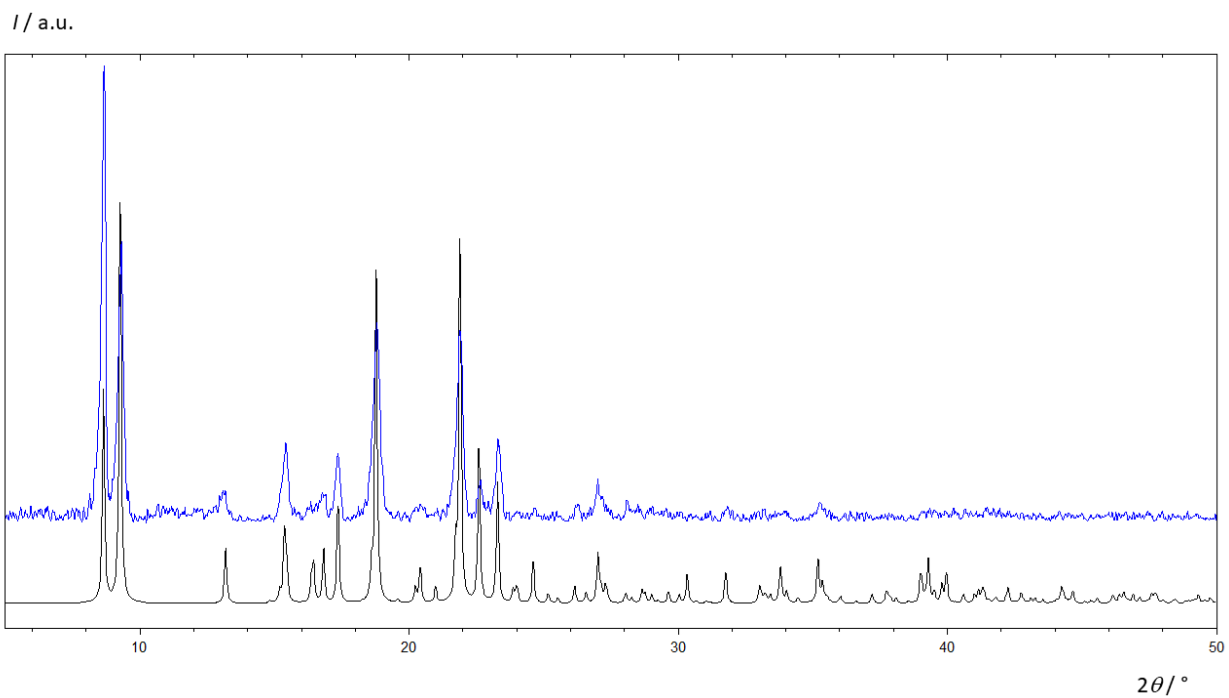


Figure S10. Experimental (**blue**) and calculated (**black**) PXR D traces of $[\text{Cu}(\text{hfac})_2(4\text{-Meoxpy})_2]$ (**4a**)

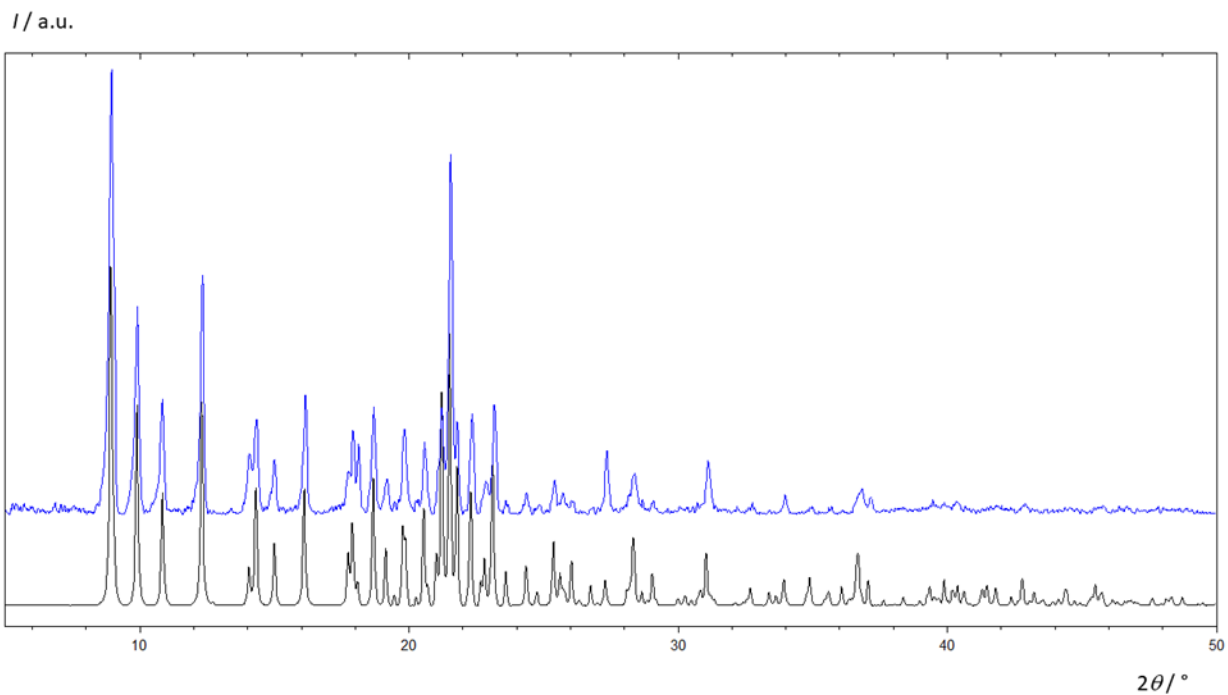


Figure S11. Experimental (**blue**) and calculated (**black**) PXRD traces of $[\text{Cu}(\text{hfac})_2(4\text{-Phoxpy})_2]$ (**5a-I**)

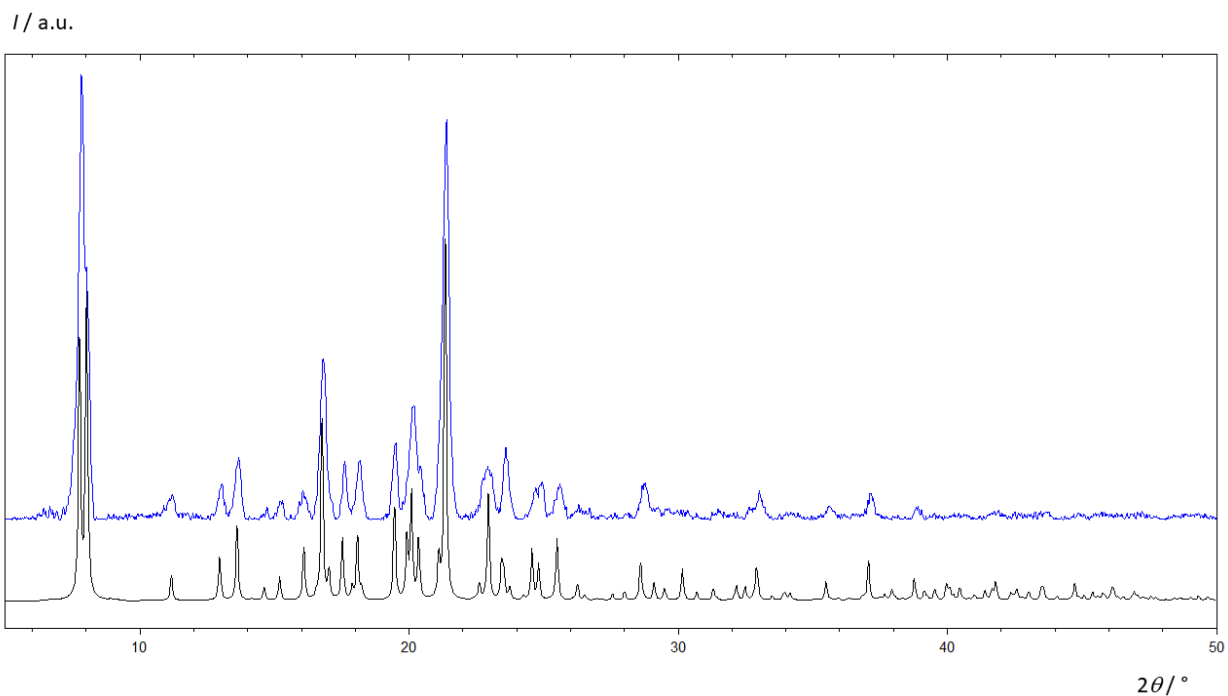


Figure S12. Experimental (**blue**) and calculated (**black**) PXRD traces of $[\text{Cu}(\text{hfac})_2(4\text{-Phoxpy})_2]$ (**5a-II**)

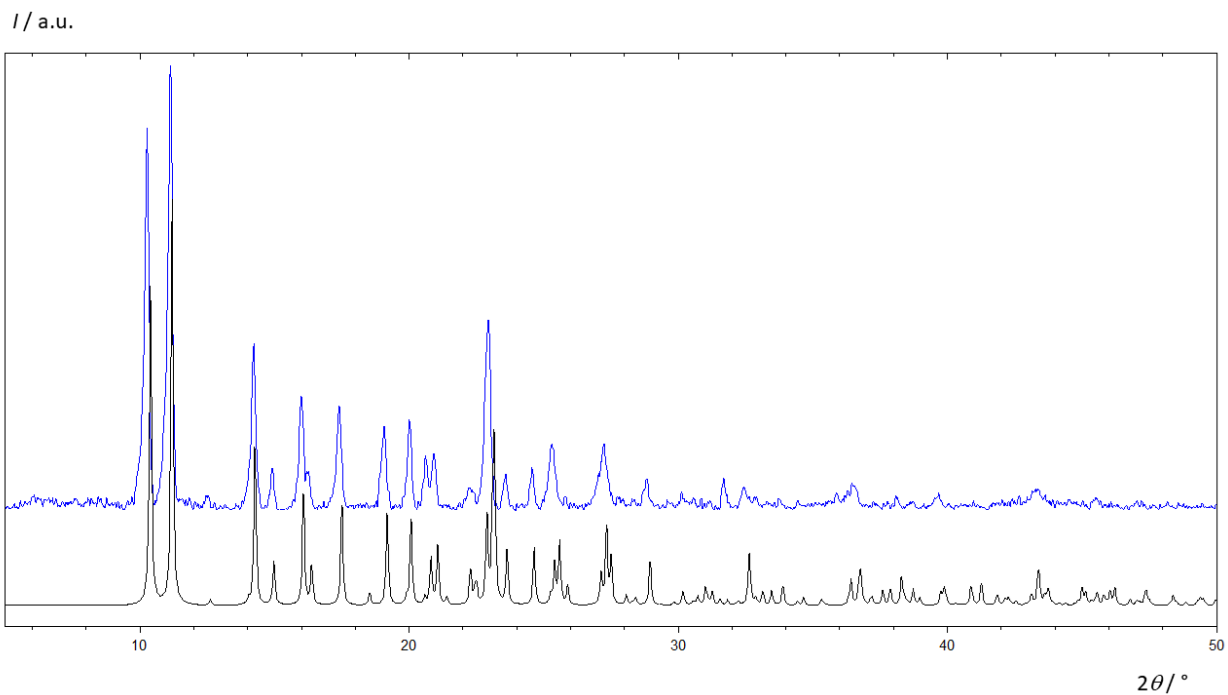


Figure S13. Experimental (**blue**) and calculated (**black**) PXR D traces of [Cu(tfac)₂(3-Meoxpy)₂] (**2b**)

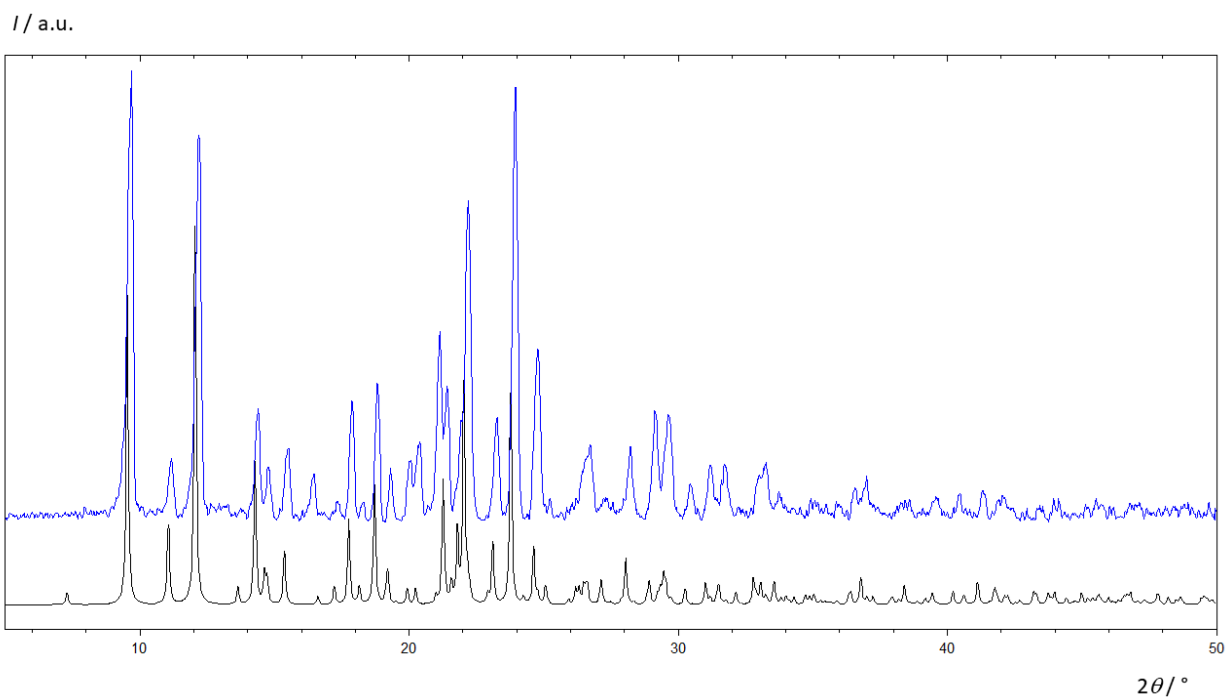


Figure S14. Experimental (**blue**) and calculated (**black**) PXR D traces of [Cu(tfac)₂(4-Hoxpy)] (**3b**)

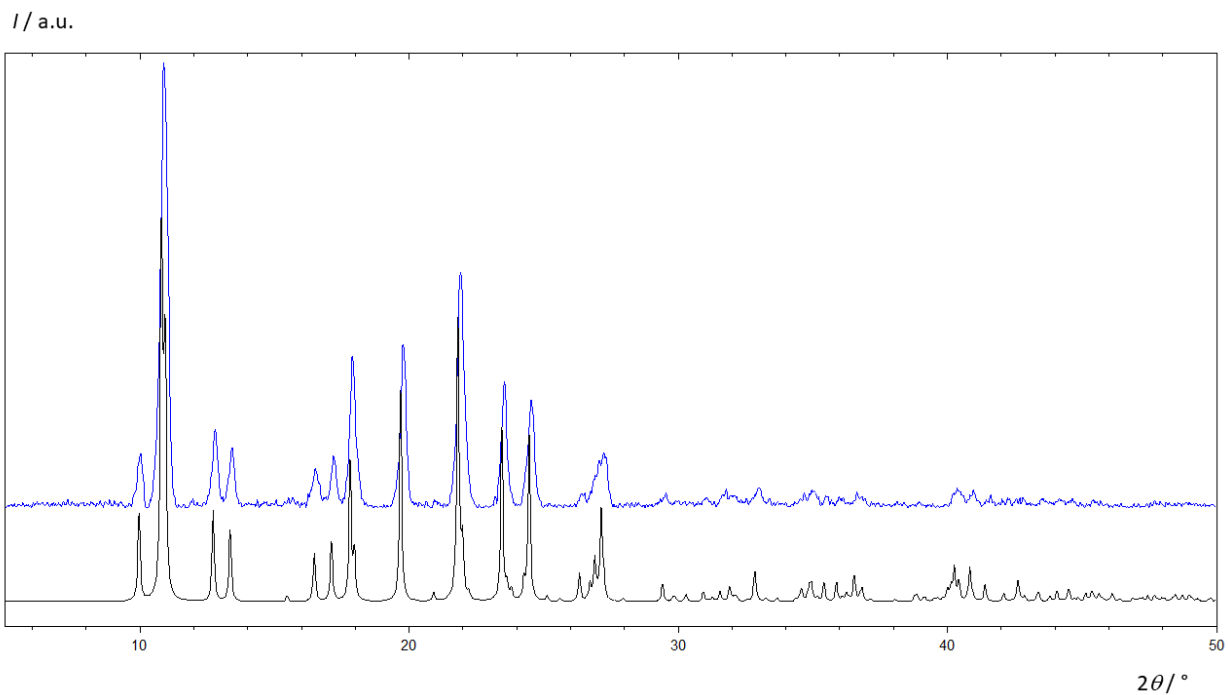


Figure S15. Experimental (**blue**) and calculated (**black**) PXR D traces of [Cu(tfac)₂(4-Meoxpy)₂] (**4b**)

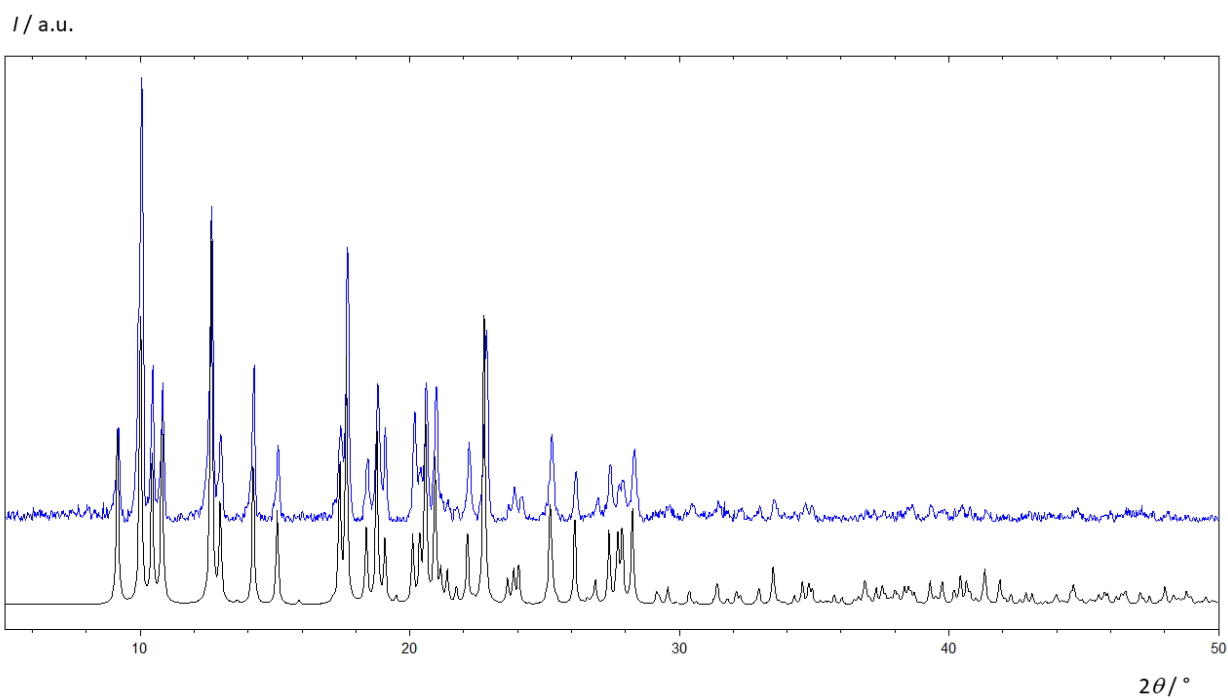


Figure S16. Experimental (**blue**) and calculated (**black**) PXR D traces of [Cu(tfac)₂(4-Phoxy)₂] (**5b**)

3. Hirshfeld surfaces

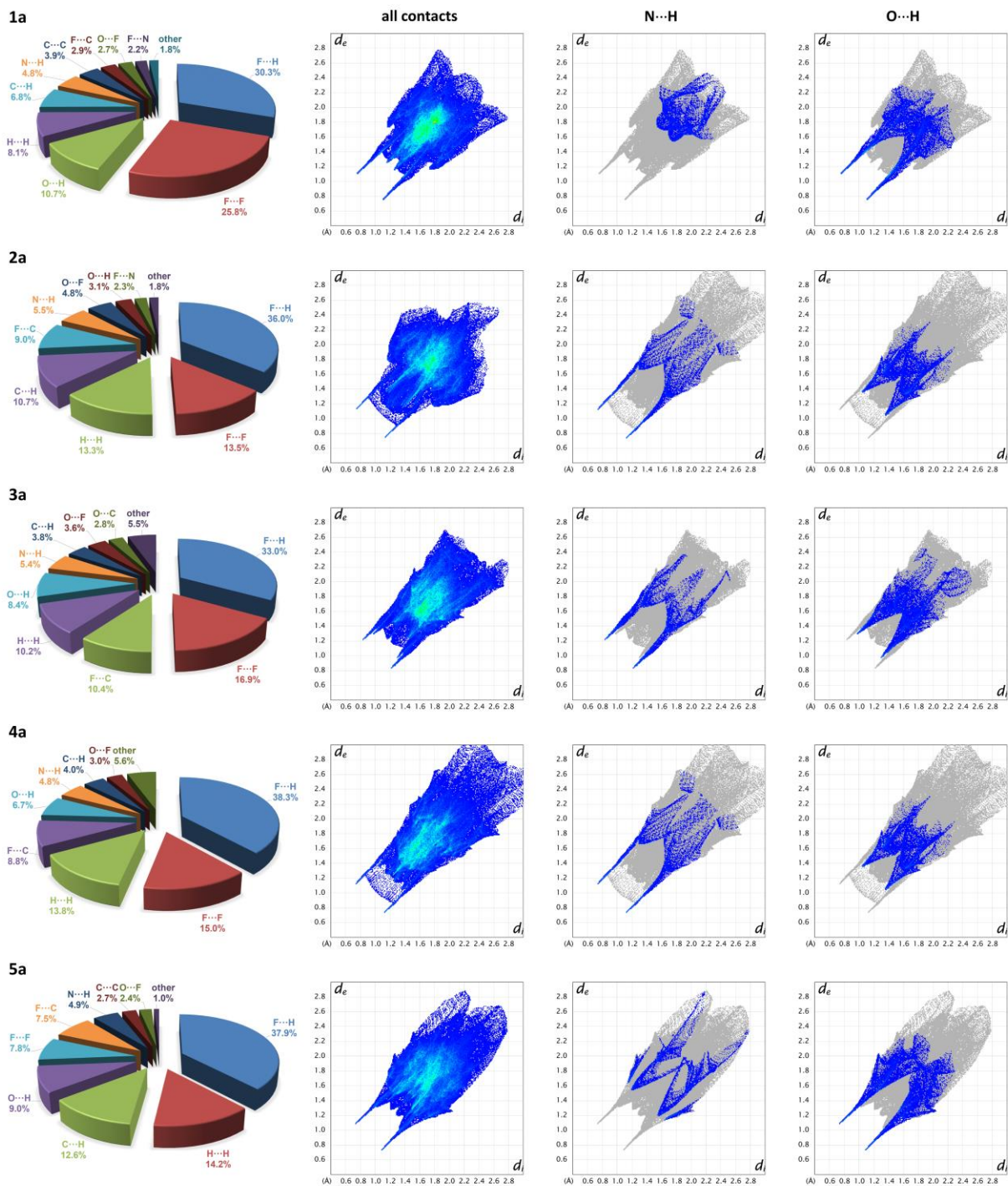


Figure S17. Percentage contributions to the Hirshfeld surface area for the selected intermolecular contacts for compounds **1a**–**5a**. Fingerprint plots for molecules of **1a**–**5a** for all contacts (left) and decomposed into contributions from N...H (middle) and O...H contacts (right).

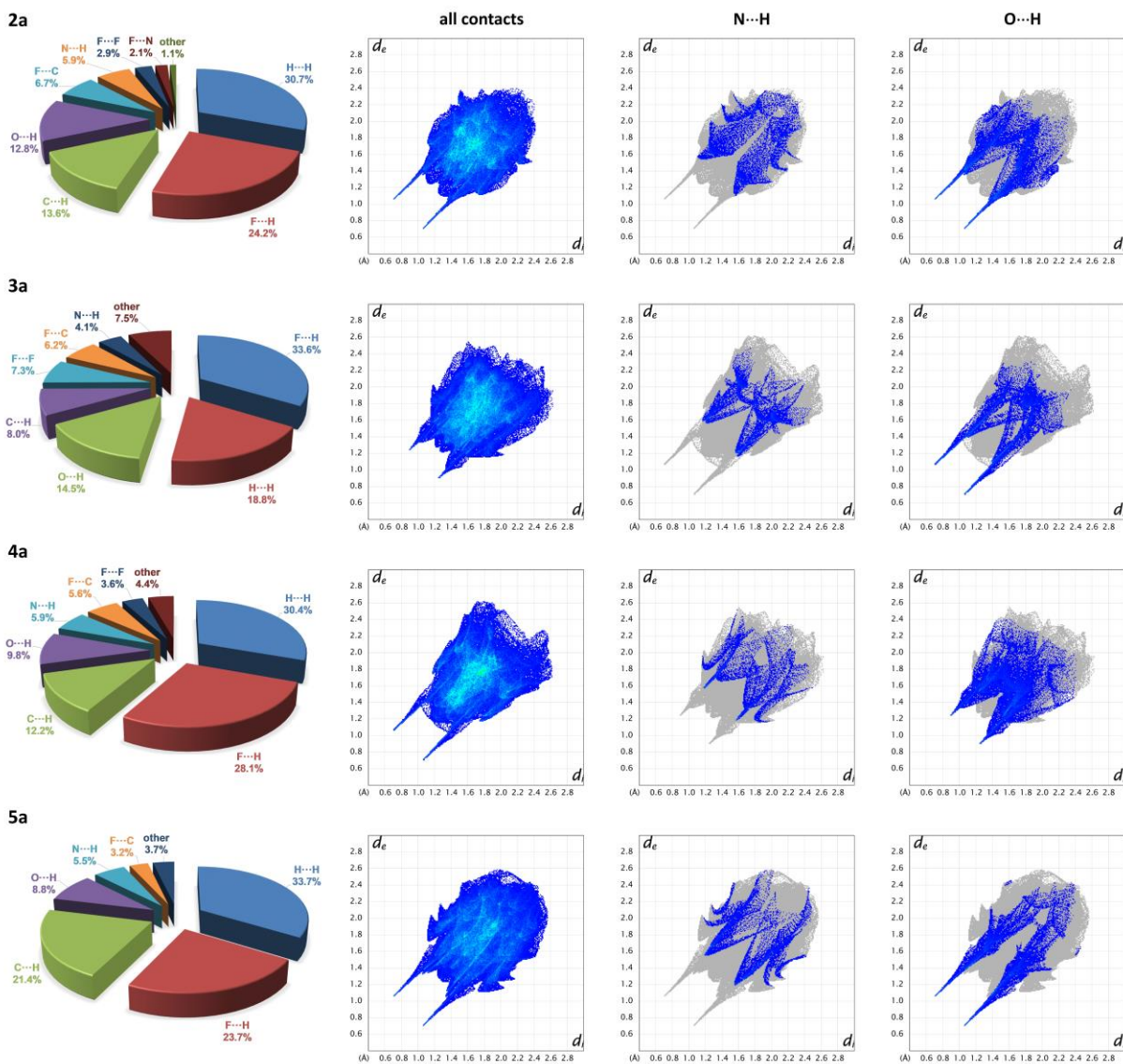


Figure S18. Percentage contributions to the Hirshfeld surface area for the selected intermolecular contacts for compounds **2b–5b**. Fingerprint plots for molecules of **2b–5b** showing all contacts (left) and decomposed into contributions from N...H (middle) and O...H (right).

4. Interaction energies of the short-range interactions

The calculated interaction energies for the primary interactions and the $C_{\text{py}}\text{-H}\cdots\text{O}_{\text{hfac}}$ hydrogen bond described in the main article already confirmed the robustness (negative ΔE_{R} and ΔE_{H}) of the materialized hydrogen-bonded links (**1a**, **2a**, **4a**, and **4b**; Table S7, Figures 14, 15, S19 and S20). Additionally, we showed that structural changes (on the molecular level, *i.e.* H/CH₃ or CF₃/CH₃ replacements) cannot significantly disrupt the materialized primary links (relatively small $\Delta\Delta E_1$, $\Delta\Delta E_2$, $\Delta\Delta E_3$, $\Delta\Delta E_5$).

This part of the theoretical study was focused on the less important, short-range interactions trying to explain their sensitivity on the specific structural changes. Charts representing the percentage of Hirshfeld surface taken by H \cdots H, H \cdots F and F \cdots F interactions, which in total exceed 50% for all the real systems (**1a**, **2a**, **4a**, and **4b**), indicate that van der Waals interactions may play a very important role in packing of molecules in the crystal structures. In addition to the dispersion forces (Figure S20) including multiple H \cdots H, H \cdots F and F \cdots F short contacts, we also analyzed stacking between planar systems of substituted py-based ligands (Figure S19).

The calculated $\Delta\Delta E$ ($\Delta\Delta E_6$ to $\Delta\Delta E_8$) values are positive, going from 20 kJ/mol in **2a**→**1a'** ($\Delta\Delta E_7$) to 61 kJ/mol in **4a**→**4b'** ($\Delta\Delta E_8$). This effect could be easily rationalized from the molecular graphs in Figures S19 and S20. The 3-Hoxpy to 3-Meoxpy replacement in **1a**→**2a'** will cause a sterical hindrance between methyl and **hfac** groups in stacked molecular pairs initiating reorganization of molecules to reach a new energy minimum. In contrast, 3-Meoxpy to 3-Hoxpy replacement in **2a**→**1a'** will leave an additional space for molecules to come much closer and establish stronger dispersion interactions between –CH₃ and –CF₃ groups (represented as green ovals in Figure S19). The exchange of **hfac** with **tfac** in **4a**→**4b'** would initiate better stabilization through H \cdots F interactions in comparison with a similar H \cdots H interactions. The same effect is observed for replacement of **tfac** in **hfac** in **4b**→**4a'** where hypothetical model with H \cdots F interaction in place of H \cdots H also shows slightly more negative ΔE_{H9} value, *i.e.* more favourable interaction.

The importance of dispersion forces is even more pronounced when 3-Hoxpy is exchanged with 3-Meoxpy in **1a**→**2a'** generating the largest positive $\Delta\Delta E_{10}$ value of 94 kJ/mol. Interestingly, the opposite exchange in **2a**→**1a'** resulted with very small $\Delta\Delta E_{11}$ value and almost negligible effect of covalent substitution. A reasonable explanation would be that the absence of the Me group in **1a** enables a tighter packing of molecules, and the system will be more sensitive to introduction of bulkier Me group preventing further tilting of pyridine-based ligands, in comparison with **2a**. The effect of **hfac** to **tfac** in **4a**→**4b'** and vice versa (**tfac** to **hfac** in **4b**→**4a'**) is almost negligible for both replacements.

A simple model used in this theoretical study indicates the robustness of the primary O–H \cdots O $_{\beta\text{-dik}}$ and O–H \cdots N $_{\text{oxime}}$ together with $C_{\text{py}}\text{-H}\cdots\text{O}_{\beta\text{-dik}}$ interactions and their resistance on covalent substitutions in the studied Cu(II) coordination complexes. In the ‘grey zone’ different supramolecular outcome could be triggered by disruption of short-range interactions due to covalent substitutions (positive $\Delta\Delta E$ values calculated for stacking and dispersion forces in **1a**, or stacking in **2a** and **4a**. In contrast, out the ‘grey zone’ short-range interactions are not significantly affected by the specific covalent substitution (small $\Delta\Delta E$ values for **4b**→**4a'** replacements). Simultaneously, disruption of the primary interactions is not influential enough to support switching of primary links (although the calculated $\Delta\Delta E_4$ is 28 kJ/mol indicating that the system

is a quite sensitive on **tfac** to **hfac** replacement, the interaction energy is still largely negative, $\Delta E_{H4} = -68$ kJ/mol, thus hampering the formation of competitive primary link).

Table S7. Complete list of interaction energies calculated for real (ΔE_R) and hypothetical (ΔE_H) models, and their differences evaluated as $\Delta\Delta E = \Delta E_H - \Delta E_R$.

Interaction	Real model		Generation of a hypothetical model		Hypothetical model		Energy difference			
	Label	ΔE_R (kJ/mol)		Replacement	Label	ΔE_H (kJ/mol)	$\Delta\Delta E$ (kJ/mol)			
primary										
O-H...N _{oxime}	2a	ΔE_{R1}	-51.7	-CH ₃ → -H (3-Meoxpy → 3-Hoxpy)	2a → 1a'	1a'	ΔE_{H1}	-44.4	$\Delta\Delta E_1$	7.3
	4a	ΔE_{R2}	-49.7	-CF ₃ → -CH ₃ (hfac → tfac)	4a → 4b'	4b'	ΔE_{H2}	-51.7	$\Delta\Delta E_2$	-2.0
O-H...O _{β-dik}	1a	ΔE_{R3}	-62.6	-H → -CH ₃ (3-Hoxpy → 3-Meoxpy)	1a → 2a'	2a'	ΔE_{H3}	-60.7	$\Delta\Delta E_3$	1.9
	4b	ΔE_{R4}	-92.6	-CH ₃ → -CF ₃ (tfac → hfac)	4b → 4a'	4a'	ΔE_{H4}	-64.8	$\Delta\Delta E_4$	27.8
secondary										
Car-H...O _{β-dik}	4a	ΔE_{R5}	-54.5	-CF ₃ → -CH ₃ (hfac → tfac)	4a → 4b'	4b'	ΔE_{H5}	-48.8	$\Delta\Delta E_5$	5.7
short-range										
stacking	1a	ΔE_{R6}	-37.2	-H → -CH ₃ (3-Hoxpy → 3-Meoxpy)	1a → 2a'	1a'	ΔE_{H6}	1.8	$\Delta\Delta E_6$	39.0
	2a	ΔE_{R7}	-45.2	-CH ₃ → -H (3-Meoxpy → 3-Hoxpy)	2a → 1a'	2a'	ΔE_{H7}	-25.4	$\Delta\Delta E_7$	19.8
	4a	ΔE_{R8}	-20.8	-CF ₃ → -CH ₃ (hfac → tfac)	4a → 4b'	4a'	ΔE_{H8}	39.9	$\Delta\Delta E_8$	60.7
	4b	ΔE_{R9}	-35.4	-CH ₃ → -CF ₃ (tfac → hfac)	4b → 4a'	4b'	ΔE_{H9}	-39.0	$\Delta\Delta E_9$	-3.6
dispersion	1a	ΔE_{R10}	-12.4	-H → -CH ₃ (3-Hoxpy → 3-Meoxpy)	1a → 2a'	1a'	ΔE_{H10}	81.9	$\Delta\Delta E_{10}$	94.3
	2a	ΔE_{R11}	-20.9	-CH ₃ → -H (3-Meoxpy → 3-Hoxpy)	2a → 1a'	2a'	ΔE_{H11}	-18.6	$\Delta\Delta E_{11}$	2.3
	4a	ΔE_{R12}	-0.4	-CF ₃ → -CH ₃ (hfac → tfac)	4a → 4b'	4a'	ΔE_{H12}	-0.9	$\Delta\Delta E_{12}$	-0.5
	4b	ΔE_{R13}	-16.0	-CH ₃ → -CF ₃ (tfac → hfac)	4b → 4a'	4b'	ΔE_{H13}	-15.4	$\Delta\Delta E_{13}$	0.6

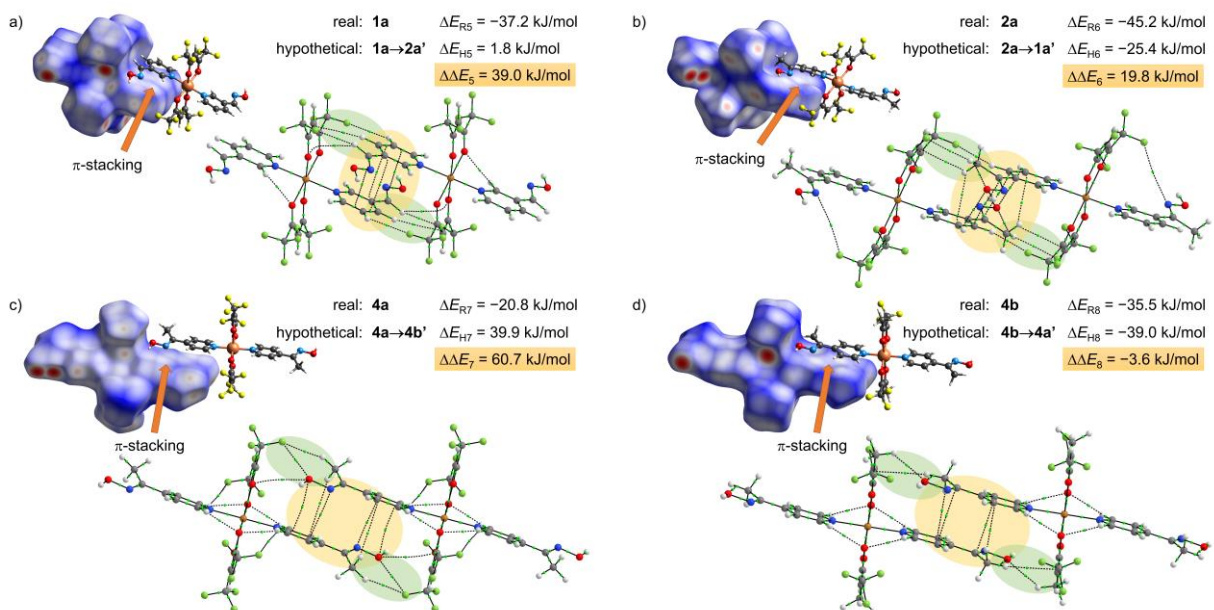


Figure S19. Theoretical models used to evaluate the stacking interaction in real (**1a**, **2a**, **4a** and **4b**) and their hypothetically generated models (**1a**→**2a'**, **2a**→**1a'**, **4a**→**4b'** and **4b**→**4a'**). For each theoretical model, top left corner shows Hirshfeld surface (plotted with normalized contact distances d_{norm}) that envelopes only one molecule from the molecular pair cut out from the crystal structure, red spots marked with orange arrows indicate shorter contacts between molecules. QTAIM generated molecular graphs (displayed in bottom left corner for each model) show multiple bond critical points between molecules; yellow ellipsoids highlight stacking interaction, green ellipsoids mark potentially disrupting contacts after replacement of ligands. Interaction energies are calculated for real (ΔE_R) and hypothetical (ΔE_H) models, and their differences evaluated as $\Delta\Delta E = \Delta E_H - \Delta E_R$.

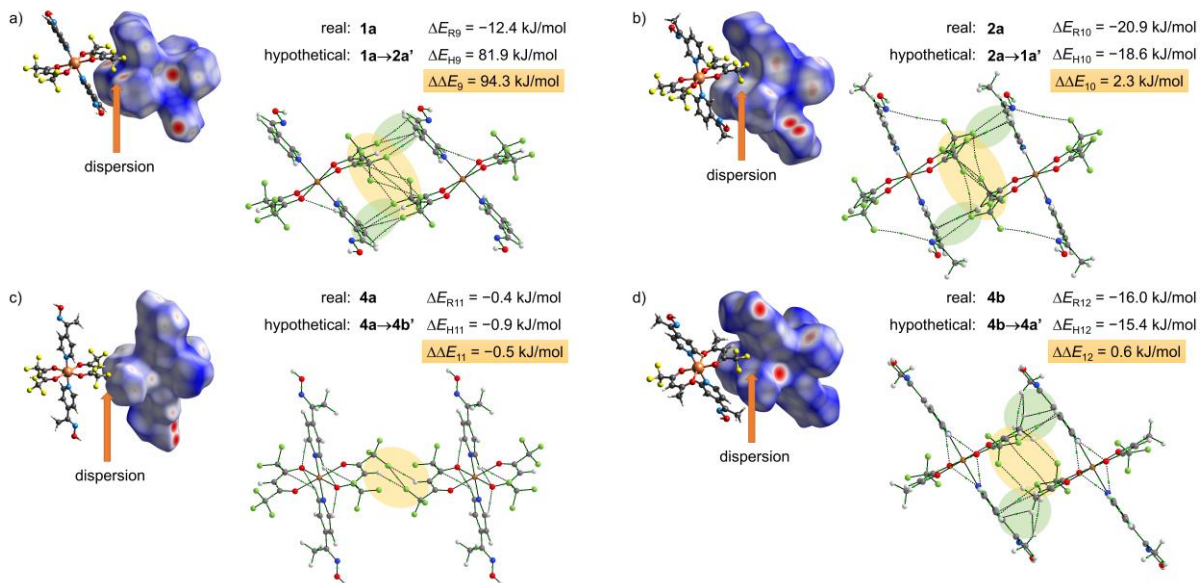


Figure S20. Theoretical models used to evaluate the short-range interaction (dispersion) in real (**1a**, **2a**, **4a** and **4b**) and their hypothetically generated models (**1a→2a'**, **2a→1a'**, **4a→4b'** and **4b→4a'**). For each theoretical model, top left corner shows Hirshfeld surface (plotted with normalized contact distances d_{norm}) that envelopes only one molecule from the molecular pair cut out from the crystal structure, red spots marked with orange arrows indicate shorter contacts between molecules. QTAIM generated molecular graphs (displayed in bottom left corner for each model) show multiple bond critical points between molecules; yellow ellipsoids highlight short-range interaction, green ellipsoids mark potentially disrupting contacts after replacement of ligands. Interaction energies are calculated for real (ΔE_R) and hypothetical (ΔE_H) models, and their differences evaluated as $\Delta\Delta E = \Delta E_H - \Delta E_R$.

5. Comparison of interaction energies calculated at different levels of theory

Table S8. Calculated interaction energies at different levels of theory for the selected molecular pairs connected by a different type of interactions used to evaluate the validity of the basis set reduction.

Interaction	Label	M06-2X/def2-SVP	M06-2X/def2-TZVP
		ΔE_R (kJ/mol)	ΔE_R (kJ/mol)
O-H \cdots N _{oxime}	2a	-51.7	-50.8
O-H \cdots O _{β-dik}	1a	-62.6	-63.8
stacking	1a	-37.2	-38.1
dispersion	1a	-12.4	-13.4